EUROPEAN ORGANIZATION FOR NUCLEAR RESEARCH

CERN–PPE/95-101

10 July 1995

Study of Prompt Photon Production in Hadronic Z^0 Decays

DELPHI Collaboration

Abstract

From a sample of 1.5 million $Z^0 \to q\overline{q}$ decays collected by the DELPHI detector during 1991, 1992 and 1993, the production cross section for isolated final state photons is measured and is compared with the $\mathcal{O}(\alpha, \alpha_s)$ matrix element calculations implemented in the EEPRAD and GNJETS Monte Carlo generators. The observed photon yield is used to derive the electroweak couplings of charge 2/3 (u-type) and charge 1/3 (d-type) quarks to the Z^0 boson. The measured values $c_{2/3} = 0.91^{+0.25}_{-0.36}$ and $c_{1/3} = 1.62^{+0.24}_{-0.17}$ are compatible with the Standard Model prediction, $c_{2/3} = 1.145$ and $c_{1/3} = 1.477$.

(To be submitted to Zeitschrift für Physik C)

P.Abreu[21], W.Adam[50], T.Adye[37], E.Agasi[31], I.Ajinenko[42], R.Aleksan[39], G.D.Alekseev[16], P.P.Allport[22], S.Almehed[24], S.J.Alvsvaag[4], U.Amaldi[9], S.Amato[47], A.Andreazza[28], M.L.Andrieux[14], P.Antilogus[25], W-D.Apel[17], Y.Arnoud[39], B.Åsman[44], J-E.Augustin[19], A.Augustinus[31], P.Baillon[9], P.Bambade[19], F.Barao[21], R.Barate[14], G.Barbiellini[46], D.Y.Bardin[16], G.J.Barker[35], A.Baroncelli[40], O.Barring[24], J.A.Barrio[26], W.Bartl[50], M.J.Bates[37], M.Battaglia[15], M.Baubillier[23], J.Baudot[39], K-H.Becks[52], M.Begalli[6], P.Beilliere[8], Yu.Belokopytov[9], A.C.Benvenuti[5], M.Berggren[47], D.Bertrand[2], F.Bianchi[45], M.Bigi[45], M.S.Bilenky[16], P.Billoir[23], D.Bloch[10], M.Blume[52], S.Blyth[35], V.Bocci[38], T.Bolognese[39], M.Bonesini[28], W.Bonivento[28], P.S.L.Booth[22], G.Borisov[42], C.Bosio[40], S.Bosworth[35], O.Botner[48], B.Bouquet[19], C.Bourdarios[9], T.J.V.Bowcock[22], M.Bozzo[13], P.Branchini[40], K.D.Brand[36], T.Brenke[52], R.A.Brenner[15], C.Bricman[2], L.Brillault[23], R.C.A.Brown[9], P.Bruckman[18], J-M.Brunet[8], L.Bugge[33], T.Buran[33], T.Burgsmueller[52], P.Buschmann[52], A.Buys[9], M.Caccia[28], M.Calvi[28], A.J.Camacho Rozas[41], T.Camporesi[9], V.Canale[38], M.Canepa[13], K.Cankocak[44], F.Cao[2], F.Carena[9], P.Carrilho[47], L.Carroll[22], C.Caso[13], M.V.Castillo Gimenez[49], A.Cattai[9], F.R.Cavallo[5], L.Cerrito[38], V.Chabaud[9], Ph.Charpentier[9], L.Chaussard[25], J.Chauveau[23], P.Checchia[36], G.A.Chelkov[16], R.Chierici[45], P.Chliapnikov[42], P.Chochula[7], V.Chorowicz[9], V.Cindro[43], P.Collins[9], J.L.Contreras[19], R.Contri[13], E.Cortina[49], G.Cosme[19], F.Cossutti[46], H.B.Crawley[1], D.Crennell[37], G.Crosetti[13], J.Cuevas Maestro[34], S.Czellar[15], E.Dahl-Jensen[29], J.Dahm[52], B.Dalmagne[19], M.Dam[33], G.Damgaard[29], A.Daum[17], P.D.Dauncey[37], M.Davenport[9], W.Da Silva[23], C.Defoix[8], G.Della Ricca[46], P.Delpierre[27], N.Demaria[35], A.De Angelis[9], H.De Boeck[2], W.De Boer[17], S.De Brabandere[2], C.De Clercq[2], C.De La Vaissiere[23], B.De Lotto[46], A.De Min[28], L.De Paula[47], C.De Saint-Jean[39], H.Dijkstra[9], L.Di Ciaccio[38], F.Djama[10], J.Dolbeau[8], M.Donszelmann[9], K.Doroba[51], M.Dracos[10], J.Drees[52], K.-A.Drees[52], M.Dris[32], Y.Dufour[8], F.Dupont[14], D.Edsall[1], R.Ehret[17], G.Eigen[4], T.Ekelof[48], G.Ekspong[44], M.Elsing[52], J-P.Engel[10], N.Ershaidat[23], B.Erzen[43], M.Espirito Santo[21], E.Falk[24], D.Fassouliotis[32], M.Feindt[9], A.Ferrer[49], T.A.Filippas[32], A.Firestone[1], P.-A.Fischer[10], H.Foeth[9], E.Fokitis[32], F.Fontanelli[13], F.Formenti[9], B.Franek[37], P.Frenkiel[8], D.C.Fries[17], A.G.Frodesen[4], R.Fruhwirth[50], F.Fulda-Quenzer[19], J.Fuster[49], A.Galloni[22], D.Gamba[45], M.Gandelman[6], C.Garcia[49], J.Garcia[41], C.Gaspar[9], U.Gasparini[36], Ph.Gavillet[9], E.N.Gazis[32], D.Gele[10], J-P.Gerber[10], L.Gerdyukov[42], M.Gibbs[22], R.Gokieli[51], B.Golob[43], G.Gopal[37], L.Gorn[1], M.Gorski[51], Yu.Gouz[42], V.Gracco[13], E.Graziani[40], G.Grosdidier[19], P.Gunnarsson[44], M.Gunther[48], J.Guy[37], U.Haedinger[17], F.Hahn[9], M.Hahn[17], S.Hahn[52], Z.Hajduk[18], A.Hallgren[48], K.Hamacher[52], W.Hao[31], F.J.Harris[35], V.Hedberg[24], R.Henriques[21], J.J.Hernandez[49], P.Herquet[2], H.Herr[9], T.L.Hessing[9], E.Higon[49], H.J.Hilke[9], T.S.Hill[1], S-O.Holmgren[44], P.J.Holt[35], D.Holthuizen[31], M.Houlden[22], J.Hrubec[50], K.Huet[2], K.Hultqvist[44], P.Ioannou[3], J.N.Jackson[22], R.Jacobsson[44], P.Jalocha[18], R.Janik[7], G.Jarlskog[24], P.Jarry[39], B.Jean-Marie[19], E.K.Johansson[44], L.Jonsson[24], P.Jonsson[24], C.Joram[9], P.Juillot[10], M.Kaiser[17], G.Kalmus[37], F.Kapusta[23], M.Karlsson[44], E.Karvelas[11], S.Katsanevas[3], E.C.Katsoufis[32], R.Keranen[15], B.A.Khomenko[16], N.N.Khovanski[16], B.King[22], N.J.Kjaer[29], H.Klein[9], A.Klovning[4], P.Kluit[31], J.H.Koehne[17], B.Koene[31], P.Kokkinias[11], M.Koratzinos[9], V.Kostioukhine[42], C.Kourkoumelis[3], O.Kouznetsov[13], P.-H.Kramer[52], M.Krammer[50], C.Kreuter[17], J.Krolikowski[51], I.Kronkvist[24], Z.Krumstein[16], W.Krupinski[18], P.Kubinec[7], W.Kucewicz[18], K.Kurvinen[15], C.Lacasta[49], I.Laktineh[25], S.Lamblot[23], J.W.Lamsa[1], L.Lanceri[46], D.W.Lane[1], P.Langefeld[52], V.Lapin[42], I.Last[22], J-P.Laugier[39], R.Lauhakangas[15], G.Leder[50], F.Ledroit[14], V.Lefebure[2], C.K.Legan[1], R.Leitner[30], Y.Lemoigne[39], J.Lemonne[2], G.Lenzen[52], V.Lepeltier[19], T.Lesiak[36], D.Liko[50], R.Lindner[52], A.Lipniacka[19], I.Lippi[36], B.Loerstad[24], M.Lokajicek[12], J.G.Loken[35], J.M.Lopez[41], A.Lopez-Fernandez[9], M.A.Lopez Aguera[41], D.Loukas[11], P.Lutz[39], L.Lyons[35], J.MacNaughton[50], G.Maehlum[17], A.Maio[21], V.Malychev[16], F.Mandl[50], J.Marco[41], B.Marechal[47], M.Margoni[36], J-C.Marin[9], C.Mariotti[40], A.Markou[11], T.Maron[52], C.Martinez-Rivero[41], F.Martinez-Vidal[49], S.Marti i Garcia[49], F.Matorras[41], C.Matteuzzi[28], G.Matthiae[38], M.Mazzucato[36], M.Mc Cubbin[9], R.Mc Kay[1], R.Mc Nulty[22], J.Medbo[48], C.Meroni[28], W.T.Meyer[1], M.Michelotto[36], E.Migliore[45], L.Mirabito[25], W.A.Mitaroff[50], U.Mjoernmark[24], T.Moa[44], R.Moeller[29], K.Moenig[9], M.R.Monge[13], P.Morettini[13], H.Mueller[17], L.M.Mundim[6], W.J.Murray[37], B.Muryn[18], G.Myatt[35], F.Naraghi[14], F.L.Navarria[5], S.Navas[49], P.Negri[28], S.Nemecek[12], W.Neumann[52], N.Neumeister[50], R.Nicolaidou[3], B.S.Nielsen[29], M.Nieuwenhuizen[31], V.Nikolaenko[10], P.Niss[44], A.Nomerotski[36], A.Normand[35], W.Oberschulte-Beckmann[17], V.Obraztsov[42], A.G.Olshevski[16], A.Onofre[21], R.Orava[15], K.Osterberg[15], A.Ouraou[39], P.Paganini[19], M.Paganoni[28], P.Pages[10], H.Palka[18], Th.D.Papadopoulou[32], L.Pape[9], C.Parkes[35], F.Parodi[13], A.Passeri[40], M.Pegoraro[36], L.Peralta[21], H.Pernegger[50], M.Pernicka[50], A.Perrotta[5], C.Petridou[46], A.Petrolini[13], H.T.Phillips[37], G.Piana[13], F.Pierre[39], M.Pimenta[21], S.Plaszczynski[19], O.Podobrin[17], M.E.Pol[6], G.Polok[18], P.Poropat[46], V.Pozdniakov[16], M.Prest[46], P.Privitera[38], N.Pukhaeva[16], A.Pullia[28], D.Radojicic[35], S.Ragazzi[28], H.Rahmani[32], J.Rames[12], P.N.Ratoff[20], A.L.Read[33], M.Reale[52], P.Rebecchi[19], N.G.Redaelli[28], D.Reid[9], P.B.Renton[35], L.K.Resvanis[3], F.Richard[19], J.Richardson[22], J.Ridky[12], G.Rinaudo[45], I.Ripp[39], A.Romero[45], I.Roncagliolo[13], P.Ronchese[36], V.Ronjin[42], L.Roos[14], E.I.Rosenberg[1], E.Rosso[9], P.Roudeau[19], T.Rovelli[5], W.Ruckstuhl[31], V.Ruhlmann-Kleider[39], A.Ruiz[41], H.Saarikko[15], Y.Sacquin[39], A.Sadovsky[16], G.Sajot[14], J.Salt[49], J.Sanchez[26], M.Sannino[13], H.Schneider[17], M.A.E.Schyns[52], G.Sciolla[45], F.Scuri[46], Y.Sedykh[16], A.M.Segar[35], A.Seitz[17], R.Sekulin[37], R.C.Shellard[6], I.Siccama[31], P.Siegrist[39], S.Simonetti[39], F.Simonetto[36], A.N.Sisakian[16], B.Sitar[7], T.B.Skaali[33], G.Smadja[25], N.Smirnov[42], O.Smirnova[16], G.R.Smith[37], R.Sosnowski[51], D.Souza-Santos[6], T.Spassov[21], E.Spiriti[40], P.Sponholz[52], S.Squarcia[13], C.Stanescu[40], S.Stapnes[33], I.Stavitski[36], K.Stepaniak[51], F.Stichelbaut[9], A.Stocchi[19], J.Strauss[50], R.Strub[10], B.Stugu[4], M.Szczekowski[51], M.Szeptycka[51], T.Tabarelli[28], J.P.Tavernet[23], O.Tchikilev[42], A.Tilquin[27], J.Timmermans[31],

L.G.Tkatchev[16], T.Todorov[10], D.Z.Toet[31], A.Tomaradze[2], B.Tome[21], L.Tortora[40], G.Transtromer[24], D.Treille[9], W.Trischuk[9], G.Tristram[8], A.Trombini[19], C.Troncon[28], A.Tsirou[9], M-L.Turluer[39], I.A.Tyapkin[16], M.Tyndel[37], S.Tzamarias[22], B.Ueberschaer[52], O.Ullaland[9], V.Uvarov[42], G.Valenti[5], E.Vallazza[9], G.W.Van Apeldoorn[31], P.Van Dam[31], W.K.Van Doninck[2], J.Van Eldik[31], N.Vassilopoulos[35], G.Vegni[28], L.Ventura[36], W.Venus[37], F.Verbeure[2], M.Verlato[36], L.S.Vertogradov[16], D.Vilanova[39], P.Vincent[25], L.Vitale[46], E.Vlasov[42], A.S.Vodopyanov[16], V.Vrba[12], H.Wahlen[52], C.Walck[44], M.Weierstall[52], P.Weilhammer[9], A.M.Wetherell[9], D.Wicke[52], J.H.Wickens[2], M.Wielers[17], G.R.Wilkinson[35], W.S.C.Williams[35], M.Winter[10], M.Witek[9], K.Woschnagg[48], K.Yip[35], O.Yushchenko[42], F.Zach[25], C.Zacharatou[24], A.Zaitsev[42], A.Zalewska[18], P.Zalewski[51], D.Zavrtanik[43], E.Zevgolatakos[11], N.I.Zimin[16], M.Zito[39], D.Zontar[43], R.Zuberi[35], G.C.Zucchelli[44], G.Zumerle[36]

[1] Ames Laboratory and Department of Physics, Iowa State University, Ames IA 50011, USA
[2] Physics Department, Univ. Instelling Antwerpen, Universiteitsplein 1, B-2610 Wilrijk, Belgium
and IIHE, ULB-VUB, Pleinlaan 2, B-1050 Brussels, Belgium
and Faculté des Sciences, Univ. de l'Etat Mons, Av. Maistriau 19, B-7000 Mons, Belgium
[3] Physics Laboratory, University of Athens, Solonos Str. 104, GR-10680 Athens, Greece
[4] Department of Physics, University of Bergen, Allégaten 55, N-5007 Bergen, Norway
[5] Dipartimento di Fisica, Università di Bologna and INFN, Via Irnerio 46, I-40126 Bologna, Italy
[6] Centro Brasileiro de Pesquisas Físicas, rua Xavier Sigaud 150, RJ-22290 Rio de Janeiro, Brazil
and Depto. de Física, Pont. Univ. Católica, C.P. 38071 RJ-22453 Rio de Janeiro, Brazil
and Inst. de Física, Univ. Estadual do Rio de Janeiro, rua São Francisco Xavier 524, Rio de Janeiro, Brazil
[7] Comenius University, Faculty of Mathematics and Physics, Mlynska Dolina, SK-84215 Bratislava, Slovakia
[8] Collège de France, Lab. de Physique Corpusculaire, IN2P3-CNRS, F-75231 Paris Cedex 05, France
[9] CERN, CH-1211 Geneva 23, Switzerland
[10] Centre de Recherche Nucléaire, IN2P3 - CNRS/ULP - BP20, F-67037 Strasbourg Cedex, France
[11] Institute of Nuclear Physics, N.C.S.R. Demokritos, P.O. Box 60228, GR-15310 Athens, Greece
[12] FZU, Inst. of Physics of the C.A.S. High Energy Physics Division, Na Slovance 2, 180 40, Praha 8, Czech Republic
[13] Dipartimento di Fisica, Università di Genova and INFN, Via Dodecaneso 33, I-16146 Genova, Italy
[14] Institut des Sciences Nucléaires, IN2P3-CNRS, Université de Grenoble 1, F-38026 Grenoble Cedex, France
[15] Research Institute for High Energy Physics, SEFT, P.O. Box 9, FIN-00014 Helsinki, Finland
[16] Joint Institute for Nuclear Research, Dubna, Head Post Office, P.O. Box 79, 101 000 Moscow, Russian Federation
[17] Institut für Experimentelle Kernphysik, Universität Karlsruhe, Postfach 6980, D-76128 Karlsruhe, Germany
[18] High Energy Physics Laboratory, Institute of Nuclear Physics, Ul. Kawiory 26a, PL-30055 Krakow 30, Poland
[19] Université de Paris-Sud, Lab. de l'Accélérateur Linéaire, IN2P3-CNRS, Bât. 200, F-91405 Orsay Cedex, France
[20] School of Physics and Materials, University of Lancaster, Lancaster LA1 4YB, UK
[21] LIP, IST, FCUL - Av. Elias Garcia, 14-1^{o}, P-1000 Lisboa Codex, Portugal
[22] Department of Physics, University of Liverpool, P.O. Box 147, Liverpool L69 3BX, UK
[23] LPNHE, IN2P3-CNRS, Universités Paris VI et VII, Tour 33 (RdC), 4 place Jussieu, F-75252 Paris Cedex 05, France
[24] Department of Physics, University of Lund, Sölvegatan 14, S-22363 Lund, Sweden
[25] Université Claude Bernard de Lyon, IPNL, IN2P3-CNRS, F-69622 Villeurbanne Cedex, France
[26] Universidad Complutense, Avda. Complutense s/n, E-28040 Madrid, Spain
[27] Univ. d'Aix - Marseille II - CPP, IN2P3-CNRS, F-13288 Marseille Cedex 09, France
[28] Dipartimento di Fisica, Università di Milano and INFN, Via Celoria 16, I-20133 Milan, Italy
[29] Niels Bohr Institute, Blegdamsvej 17, DK-2100 Copenhagen 0, Denmark
[30] NC, Nuclear Centre of MFF, Charles University, Areal MFF, V Holesovickach 2, 180 00, Praha 8, Czech Republic
[31] NIKHEF-H, Postbus 41882, NL-1009 DB Amsterdam, The Netherlands
[32] National Technical University, Physics Department, Zografou Campus, GR-15773 Athens, Greece
[33] Physics Department, University of Oslo, Blindern, N-1000 Oslo 3, Norway
[34] Dpto. Fisica, Univ. Oviedo, C/P. Pérez Casas, S/N-33006 Oviedo, Spain
[35] Department of Physics, University of Oxford, Keble Road, Oxford OX1 3RH, UK
[36] Dipartimento di Fisica, Università di Padova and INFN, Via Marzolo 8, I-35131 Padua, Italy
[37] Rutherford Appleton Laboratory, Chilton, Didcot OX11 OQX, UK
[38] Dipartimento di Fisica, Università di Roma II and INFN, Tor Vergata, I-00173 Rome, Italy
[39] Centre d'Etudes de Saclay, DSM/DAPNIA, F-91191 Gif-sur-Yvette Cedex, France
[40] Istituto Superiore di Sanità, Ist. Naz. di Fisica Nucl. (INFN), Viale Regina Elena 299, I-00161 Rome, Italy
[41] C.E.A.F.M., C.S.I.C. - Univ. Cantabria, Avda. los Castros, S/N-39006 Santander, Spain, (CICYT-AEN93-0832)
[42] Inst. for High Energy Physics, Serpukov P.O. Box 35, Protvino, (Moscow Region), Russian Federation
[43] J. Stefan Institute and Department of Physics, University of Ljubljana, Jamova 39, SI-61000 Ljubljana, Slovenia
[44] Fysikum, Stockholm University, Box 6730, S-113 85 Stockholm, Sweden
[45] Dipartimento di Fisica Sperimentale, Università di Torino and INFN, Via P. Giuria 1, I-10125 Turin, Italy
[46] Dipartimento di Fisica, Università di Trieste and INFN, Via A. Valerio 2, I-34127 Trieste, Italy
and Istituto di Fisica, Università di Udine, I-33100 Udine, Italy
[47] Univ. Federal do Rio de Janeiro, C.P. 68528 Cidade Univ., Ilha do Fundão BR-21945-970 Rio de Janeiro, Brazil
[48] Department of Radiation Sciences, University of Uppsala, P.O. Box 535, S-751 21 Uppsala, Sweden
[49] IFIC, Valencia-CSIC, and D.F.A.M.N., U. de Valencia, Avda. Dr. Moliner 50, E-46100 Burjassot (Valencia), Spain
[50] Institut für Hochenergiephysik, Österr. Akad. d. Wissensch., Nikolsdorfergasse 18, A-1050 Vienna, Austria
[51] Inst. Nuclear Studies and University of Warsaw, Ul. Hoza 69, PL-00681 Warsaw, Poland
[52] Fachbereich Physik, University of Wuppertal, Postfach 100 127, D-42097 Wuppertal 1, Germany

1 Introduction

In $e^+e^- \to q\overline{q}$ events, high energy photons can be produced either by prompt radiation from the initial state and the final state particles, or from the decay of short lived hadrons such as $\pi^0 \to \gamma\gamma$ or $\eta \to \gamma\gamma$ (non-prompt radiation). As energetic π^0's are usually imbedded in a jet, i.e. surrounded by other hadronic fragments, a relatively clean sample of prompt-photon candidates can be obtained by requiring a minimum isolation angle with respect to the hadronic jets [1]. At the peak of the Z^0 resonance, prompt radiation from the initial state (ISR) is highly suppressed [2]. This makes LEP the ideal place for the study of final state radiation (FSR), which can be compared with the Standard Model predictions. Previous studies of the production of energetic prompt photons in hadronic Z^0 decays at LEP are described in references [3–6].

In QCD the inclusive cross section for emitting final state photons in $e^+e^- \to q\overline{q}$ events can be expressed as the convolution of two terms [7]:

$$\frac{d\sigma_\gamma}{dE_\gamma} = \sum_{p=q,\overline{q},g,\gamma} \int_0^{\sqrt{s}/2} dE_p \int_0^1 dz \frac{d\hat{\sigma}^p}{dE_p}(E_p, \mu, Q^2, \alpha_s(\mu)) D_p^\gamma(z,\mu)\delta(E_\gamma - zE_p) \qquad (1)$$

where $\alpha_s(\mu)$ is the strong coupling constant at the ultraviolet renormalization scale μ and Q^2 is the factorization scale. In eqn. (1) $d\hat{\sigma}^p/dE_p(E_p, \mu, Q^2, \alpha_s(\mu))$ represents the perturbative hard scattering cross section for producing a parton p with energy E_p, while $D_p^\gamma(z,\mu)$ is the parton-to-photon fragmentation function, which describes the probability for the parton p to fragment into a photon with fractional energy $z = E_\gamma/E_p$.

According to eqn. (1) final state photons can originate either in the perturbative regime through the $d\hat{\sigma}^p$ term, or in the parton-to-photon fragmentation ($D_p^\gamma(z,\mu)$) through non-perturbative mechanisms such as Vector Meson Dominance coupling. However the non-perturbative contribution, which is sometimes referred to as the 'anomalous component' [7], is suppressed for *isolated* photon emission. For this reason it is believed that the analysis of isolated prompt photons can provide a clean test for the *perturbative* prediction of QCD [2,7–11]. The advantage of studying photon emission (as compared with gluon emission) in QCD derives from the the fact that prompt photons do not participate, to first approximation, in the hadronization process, they compete directly with gluon emission, and they may be directly detected in the experimental apparatus.

In the following, the FSR photon yield measured in the multi-hadronic sample collected by DELPHI in 1991, 1992 and 1993 is compared with exact $\mathcal{O}(\alpha, \alpha_s)$ matrix element (ME) calculations as implemented in the EEPRAD [11] and GNJETS [12] Monte Carlo generators. A previous comparison of the DELPHI data with the predictions of the JETSET 7.3 parton shower (PS) model [13] for final state radiation can be found in reference [4]. As isolated photon emission is a hard process, exact matrix element calculations are believed to be more reliable than predictions based on the parton shower approach [13–15]. The only uses made here of a parton shower model, specifically JETSET 7.3 PS, are aimed at determining the background contaminations from non-prompt photons passing the selection criteria and the corrections needed to recover the differential cross sections for photon emission at the parton level from the experimental hadron distributions. In fact neither GNJETS nor EEPRAD include any simulation of the fragmentation process. The use of two different ME Monte Carlo generators (EEPRAD and GNJETS) is due to the slightly different mechanisms with which they solve the problems related to the occurrence of divergences in the gluon-quark soft and colinear singularity [10].

In the electroweak sector, a measurement of the final state photon emission rate can also be used to determine the electroweak couplings of u-type and d-type quarks to the

Z^0 boson. Specifically, while the rate of Z^0 decay into hadrons, which is well-determined experimentally from the hadronic width of the Z^0 , is proportional to the numbers of u-type and d-type quarks, the rate of final state radiation is also proportional, in lowest order, to the squares of the electric charges of the primary quarks. Since the two linear combinations are different, the couplings may be extracted separately [16]. The measurement of the electroweak couplings will be discussed in detail in Section 8.

2 The DELPHI Detector

Features of the DELPHI apparatus relevant for the analysis of multihadronic final states are detailed in reference [17]. The present analysis relies on the information provided by the three cylindrical tracking detectors (Inner Detector, Time Projection Chamber (TPC), and Outer Detector), by the microvertex chamber for more precise tracking, by the forward tracking chambers A and B, and by the electromagnetic calorimeters HPC and FEMC for photon detection, all operating in a 1.2 T magnetic field.

The Inner Detector and TPC each cover the angular range $20^\circ < \theta < 160^\circ$, where θ is the polar angle with respect to the beam axis, and the Outer Detector covers the range $43^\circ < \theta < 137^\circ$. The chambers A and B provide the tracking in the forward region, with acceptance $11^\circ < \theta < 33^\circ$ and $147^\circ < \theta < 169^\circ$ in polar angle.

Energetic isolated photons are detected in the barrel electromagnetic calorimeter, called the High-density Projection Chamber (HPC), and in the Forward Electromagnetic Calorimeter (FEMC).

The HPC is a gas sampling calorimeter which provides complete three-dimensional charge information in the manner of a time-projection chamber. It subtends the angular range $41^\circ < \theta < 139^\circ$, and is mounted directly inside the 5.2-meter (inner diameter) superconducting solenoid of DELPHI. The HPC consists of 144 modules arranged in 24 azimuthal sectors, where each sector consists of six modules along the beam axis. Each module consists of 41 layers of lead radiator totalling about 17 radiation lengths, interspersed with 40 gas sampling slots containing a mixture of argon and methane gases. Charge due to ionization produced in the electromagnetic showers drifts along the beam (z) axis in parallel electric and magnetic fields, and is read out via a grid of cathode pads which provides 9 samplings along the shower axis. The 15 MHz sampling frequency corresponds to a cell size of 3.5 mm along the beam axis, with a spatial resolution varying between 1.3 and 3.1 mm according to the polar angle. The granularity in the azimuthal angle (ϕ) is about 20 mrad. The HPC has been described in the literature [18] as have the readout electronics [19]. The energy resolution of the HPC at 45 GeV as determined from a study of the Bhabha events is 6%.

The DELPHI Forward Electromagnetic Calorimeter (FEMC) [20] subtends a polar angle $10^\circ < \theta < 37^\circ$ and $143^\circ < \theta < 170^\circ$. It consists of two 5 m diameter disks with a total of 9064 lead glass blocks in the form of truncated pyramids. The lead glass counters (20 radiation length deep, 5×5 cm^2, $\sim 1^\circ \times 1^\circ$) are read out with vacuum photodiodes, giving an average gain of 12, which is reduced by 30% in the 1.2 T magnetic field. Test beam results showed an energy resolution of $(\sigma/E)^2 = (0.35\% + 5\%/\sqrt{E})^2 + (4\%/E)^2$, with E in GeV, the last term being due to amplification noise. In DELPHI the FEMC energy resolution is degraded due to about two radiation lengths of material in front of the calorimeter. Bhabha showers at 45 GeV are measured with $(\sigma/\mathrm{E}) = 4\%$.

3 Event selection

Events with isolated final state photons are extracted from a sample of 1,483,906 multihadronic Z^0 decays. The hadronic event selection is based on large charged multiplicity ($N_{ch} \geq 5$) and high visible energy ($E_{vis} \geq 20\%\sqrt{s}$). In addition, the condition $30^\circ \leq \theta_{thrust} \leq 150^\circ$ is imposed, where θ_{thrust} is the angle between the thrust axis and the beam direction. These criteria correspond to a total efficiency of $(85.2 \pm 0.1)\%$ [$(94.9 \pm 0.1)\%$ without the requirement on the thrust axis] for hadronic Z^0 decays, with a $Z^0 \to \tau^+\tau^-$ contamination of $(0.4 \pm 0.1)\%$. The data were recorded mostly at a center of mass energy of $\sqrt{s} = 91.2$ GeV, with a $\sim$ 20% fraction collected off-peak in the range $88.4 \leq \sqrt{s} \leq 93.6$ GeV.

Events with hard final state radiation are selected by requiring the presence of an energetic neutral shower in an electromagnetic calorimeter, HPC or FEMC, satisfying the following requirements:

- energy $E_\gamma > 5.5$ GeV,
- polar angle $25^\circ < \theta_\gamma < 155^\circ$,
- minimum isolation angle of 20° with respect to any reconstructed charged or neutral particle with energy $E > 500$ MeV.

When the conditions are satisfied by two or more photons in a single event only the most energetic photon is considered in this analysis.

As discussed above, the minimum isolation condition strongly reduces the non-prompt background, while the cut on θ_γ supresses the ISR contamination which is concentrated at small polar angles.

In addition, the neutral cluster must be identified as a single electromagnetic deposit according to the criteria described in the next section. This requirement reduces the background from hadronic showers and from unresolved photon pairs generated in π^0 decays.

4 Photon identification

In the HPC, genuine single photon showers are identified through the parameter W_{HPC}, where W_{HPC} is defined as:

$$W_{HPC} = \sqrt{\sum_i X_i \cdot (\Delta\theta_i)^2}, \tag{2}$$

in which X_i is the fraction of energy associated to each cluster reconstructed in the shower and $\Delta\theta_i$ is its separation in polar angle from the shower starting point expressed in degrees. The sum runs over the clusters reconstructed in the first three sampling layers along the shower axis. Because of its definition, the W_{HPC} parameter provides an estimate of the cluster spread in the transverse plane, which is expected to be larger for showers produced by partially overlapping photons.

The distribution of the W_{HPC} parameter for the selected events is shown in fig. 1. The expectations from simulation, based on JETSET 7.3 PS and on the DELPHI detector simulation program DELSIM [21], are superimposed on the data. Data and simulation are each normalized to the total luminosity. Genuine single photon showers are identified by the condition $W_{HPC} < 1$.

The combined efficiency after the cuts, as derived from simulation, is ε_γ^{HPC}=(81.1±0.6 (stat.))% for isolated photons with energy larger than 5.5 GeV. The rejection factors against non-prompt photons and non-electromagnetic showers (later called neutral hadrons) correspond to 1.8 and 6.7 respectively. For the non-prompt photon background the rejection factor is computed for all photons produced in $Z^0 \to q\overline{q}$ decays whose origin is not final state radiation. Consequently this background also includes the irreducible contamination from isolated non-overlapping photons produced in meson decays.

In the FEMC the photon identification criterion relies on the W_{FEMC} parameter which is defined as:

$$W_{FEMC} = \sum_{i=1}^{4} X_i, \tag{3}$$

where X_i is the fraction of energy associated to the i^{th} lead glass block and the sum runs over the set of four blocks centered around the shower barycenter. Isolated final state photons are selected by the condition $W_{FEMC} > 0.95$, with an efficiency of (90.1±0.8(stat.))%. The rejection factors against the non-prompt and the non-electromagnetic backgrounds are 1.2 and 2.6 respectively. The fraction of events with the isolated photon reconstructed in the FEMC is about 8% of the selected FSR sample.

A further large improvement in background rejection is obtained by comparing in each event the energy measured in the electromagnetic calorimeters for the isolated neutral shower and the estimate obtained by means of a rescaling procedure which is based on the following steps:

1. All particles (neutrals and charged) except the isolated photon are clustered into two jets according to the K_T (also called 'Durham') algorithm [22]. In the K_T algorithm, pairs of 'particles' are iteratively recombined into jets beginning with the pair with the lowest value of a scaled invariant mass variable, y_{ij}, given by

$$y_{ij} = \frac{2\min(E_i^2, E_j^2)(1-\cos\theta_{ij})}{E_{vis}^2}, \tag{4}$$

   where E_i is the energy of 'particle' i and θ_{ij} is the angle between 'particles' i and j. The 'particles' may be individual particles or recombined 'jets'.
2. Momentum conservation is imposed on the event in order to calculate the energies of the photon and the jets (assumed to be massless), in terms of their observed angles and the total center-of-mass energy. If the photon and the jet directions are identified with vectors i, j and k, then the calculated energies are given by the formula

$$E_i^{calc} = \frac{|\sin\theta_{jk}|}{(|\sin\theta_{ij}| + |\sin\theta_{ik}| + |\sin\theta_{kj}|)}\sqrt{s}, \tag{5}$$

   where θ_{ij} is the angle between vectors i and j and $\sqrt{s}$ is the centre-of-mass energy. Non-planar events are rejected by demanding that the sum of the three angles θ_{ij} be larger than 345°.

The events in which the difference between the calculated and the measured photon energies $(E_\gamma^{calc} - E_\gamma^{meas})$ is larger than $+1.3\sigma$ or smaller than -2.5σ, where σ is the combined energy resolution, are discarded. This reduces not only the contamination from long-lived neutral hadrons, for which E_γ^{calc} is normally much larger than E_γ^{meas}, but also that of non-prompt radiation. This is because most of the observed non-prompt background is in fact accompanied by hadronic fragments not seen by the apparatus (or not considered in the analysis). In such cases the imposition of momentum conservation

tends to increase the energy ascribed to the photon in order to correct for the momentum imbalance produced by the missing particles. This also explains the use of an asymmetric cut. With this method the backgrounds from non-prompt photons and neutral hadrons passing the selection criteria are reduced by factors 2.0 and 2.8 respectively, while keeping 83.7% of the FSR photons.

The systematic uncertainty associated with the photon identification criteria is estimated from the data in a background sample of non-isolated photons detected in Z^0 multihadronic decays and in a signal sample of isolated showers detected in Z^0 leptonic decays. This uncertainty translates into a $\pm 3.0\%$ uncertainty on the FSR cross section.

5 Residual background evaluation

A total of 3147 radiative hadronic Z^0 events pass all selection criteria described in the previous sections. In order to extract the FSR cross section all the residual background contaminations must be evaluated and subtracted. These consist primarily of:

- initial state radiation,
- fragmentation background, that is non-prompt photons from light meson decay ($\pi^0 \to \gamma\gamma$, $\eta \to \gamma\gamma$) or long-lived neutral hadrons faking electromagnetic deposits in the calorimeters,
- isolated FSR photons in $Z^0 \to \tau^+\tau^-$ decays.

Each is described in turn below.

5.1 ISR background

An estimate of the ISR background contribution to the selected sample has been obtained by interfacing the DYMU3 generator [23] with the JETSET 7.3 PS program in the generation of over two million multihadronic events. DYMU3 can simulate initial state radiation up to second order QED. According to DYMU3 predictions, the ISR contamination is $(8.1 \pm 0.5)\%$. However the production of hard initial state radiation also has been studied directly in the data by analysing highly isolated photons with energy $E_\gamma > 3.5$ GeV emitted at angles smaller than 20° from the beam axis. The analysis of ISR makes use of the Forward Electromagnetic Calorimeter (FEMC) and of the Small Angle Tagger (SAT)[17], the DELPHI luminosity monitor. The data show that the predictions from the simulation must be rescaled by the factor 0.84 with an uncertainty of $\pm 14\%$(stat.) $\pm\, 7\%$(syst.), which translates into a $\pm 1.3\%$ systematic uncertainty on the FSR cross section. The large uncertainty on the ISR measurement is due to the extreme hardness of the cuts required to select the rare events with visible initial state radiation and by the possible contamination of low energy particles from the LEP beam halo.

5.2 Fragmentation background

The fragmentation background consists of secondary photons from light meson decay and of long lived neutral hadrons.

According to the Lund string model [24] as implemented in JETSET 7.3 PS, the fragmentation background amounts to $(14.9 \pm 0.6)\%$ of the selected events. This estimate is also checked with the data by selecting two independent background samples:

1. the first sample consists of non-completely isolated photons, i.e. photons for which one secondary neutral shower is reconstructed within a cone with 20° half-angle around the photon direction;
2. the second sample is based on the events with a signal in the electromagnetic calorimeters satisfying all isolation criteria but which are anti-tagged by the photon identification algorithm, i.e. that are not true single photons.

The ratios between the number of real and simulated events in the two samples are shown in fig. 2 as a function of the shower energy. The figure shows that in both cases JETSET 7.3 PS does not correctly reproduce the background yield, which is underestimated at low energy and slightly overestimated at high energy.

The contamination from fragmentation processes in the simulation is therefore rescaled as a function of energy according to the average of the two superimposed histograms of fig. 2. As a result the estimate of the overall background contamination is increased to $(17.0 \pm 0.7)\%$.

A systematic uncertainty equal to half the difference between the two estimates of fig. 2 is assumed for the background subtraction. This translates into a $\pm 2.8\%$ uncertainty on the measurement of the FSR cross section.

5.3 $Z^0 \to \tau^+\tau^-\gamma$ background

As discussed above, the hadronic selection criteria imply a 0.4% background contamination from $Z^0 \to \tau^+\tau^-$ decays. However, this estimate must be re-evaluated after the selection of events with isolated photons because of the different coupling of quarks and τ leptons to the photon. According to simulation [25] the $Z^0 \to \tau^+\tau^-$ contamination in the final sample reaches $(1.9 \pm 0.3)\%$, i.e. a factor ~ 4.8 larger than in the multi-hadronic sample, in agreement with what is naively expected by comparing the average electric charge of quarks in Z^0 decays with the τ lepton charge:

$$\frac{e_\tau^2}{< e_q^2 >} \sim 4.5 \tag{6}$$

The systematic uncertainty in the $Z^0 \to \tau^+\tau^-\gamma$ background is assumed to be negligible.

6 Data analysis

The photon energy distribution for the final sample is shown in fig. 3, where the data are compared with JETSET 7.3 PS predictions, after subtracting the small $Z^0 \to \tau^+\tau^-\gamma$ background and rescaling the fragmentation background predicted by JETSET according to the procedure described in the previous section. The uncertainties shown in fig. 3 are statistical only.

A systematic uncertainty of $\pm 2\%$ is assigned globally to the requirements concerning the photon minimum energy and isolation criterion. This estimate is based on the possible deviation from linearity affecting the evaluation of the photon energy in the calorimeters and on the level of accuracy with which low energy showers are reproduced in the simulation. An additional uncertainty of $\pm 3.4\%$ is also assigned for the degree of reproducibility of the material in front of the calorimeters. As already stated other important sources of systematic uncertainty are the photon identification algorithm (3.0%) and the background subtraction (2.8% for non prompt radiation, 1.3% for ISR). Summing

up all separate contributions in quadrature, the total systematic uncertainty affecting the selection of FSR photons in the data is $\pm 5.8\%$.

Despite the background rescaling, the data still show a $(18 \pm 4(\text{stat.}) \pm 6(\text{syst.}))\%$ excess with respect to JETSET 7.3 PS predictions for isolated final state photons. This disagreement is heavily concentrated at the low energy region of the photon spectrum, but is also true in the higher energy region around 32-40 GeV.

In order to compare the data with $\mathcal{O}(\alpha, \alpha_s)$ matrix element predictions, a jet-finding algorithm is applied to the selected FSR events. The jet rate distributions are then corrected for acceptance and fragmentation effects and are compared with the theoretical predictions as a function of the jet resolution parameter. The procedure adopted in the analysis is described in detail in the following sections.

6.1 Jet reconstruction

For each of the selected events the following three-step procedure is applied:

1. The isolated photon is first removed from the event.
2. The K_T jet-finding algorithm is applied to the remaining particles using a particular value of the resolution parameter y, that is all particles are recombined into jets until the condition
$$y_{ij} > y, \tag{7}$$
where y_{ij} is the scaled mass defined in eqn. (4), is satisfied by all pairs of particles.
3. The photon is reintroduced into the event, and for the same value of y the K_T algorithm is applied to the photon and to the hadronic jets. Those events in which the photon remains resolved from the hadronic jets are classified as FSR events with 1, 2 or ≥ 3 hadronic jets. Those in which the photon is associated with a hadronic jet are rejected.

For the comparison with matrix element predictions, values of y in the range $0.01 \leq y \leq 0.20$ are considered. The region $y < 0.01$ is excluded due to the presence of large 3-jet (and 4-jet) fractions, which imply non-negligible higher order QCD corrections. Values of y above 0.20 are not considered because they show large sensitivity to the photon-quark singularity (colinear production) in the matrix element [10].

In order to be compared with the $\mathcal{O}(\alpha, \alpha_s)$ matrix element predictions, the observed fractions of events with an isolated photon plus 1,2 or ≥ 3 hadronic jets,

$$f_n^{exp}(y) = \frac{\Gamma(Z^0 \to \gamma + \text{n jets})(y)}{\Gamma(Z^0 \to q\overline{q})}, \quad n = 1, 2, 3, \tag{8}$$

are corrected for efficiency and fragmentation effects as follows.

6.2 Correction procedure

The correction procedure applied to the observed $f_n^{exp}(y)$ distributions is based on two separate steps:

1. The first correction (*acceptance* correction) accounts for the limited acceptance and for the finite resolution of the experimental apparatus.
2. The second correction (*fragmentation* correction) represents an estimate of the distortions introduced by the hadronization process and translates the hadron distributions of the experimental data into the few-parton language of the matrix element approach.

6.2.1 Acceptance correction

For the acceptance correction ($\delta^{(n)}_{acc}(y)$) the DELPHI detector simulation package [21] is used, together with the reference sample of hadronic Z^0 decays generated by JETSET 7.3 PS. In more detail, the correction factor is defined as the ratio

$$\delta^{(n)}_{acc}(y) = \frac{N^{(n)}_{had}(y)}{N^{(n)}_{exp}(y)}. \tag{9}$$

In eqn. (9) $N^{(n)}_{had}(y)$ is the number of γ+n-jet events generated in the full 4π solid angle, while $N^{(n)}_{exp}(y)$ is the number of γ+n-jet events reconstructed after passing through the DELPHI detector simulation package. In the definition of $N^{(n)}_{had}(y)$ the photon is assumed to be isolated if the total energy of all particles generated in a 20° cone around the photon is less than 500 MeV.

The comparison between DELPHI data (after applying the acceptance correction) and the JETSET 7.3 PS model is shown in fig. 4. The figure shows that the absolute jet rates seem to be well reproduced by the JETSET parton shower model once the non-prompt background is rescaled according to the procedure described in Section 5.2. In fact the excess of low energy isolated photons in the data reported in Section 6 disappears once the photon is required to be isolated from the hadronic jets by a cut in invariant mass.

6.2.2 Fragmentation correction

Similarly to the acceptance correction, the fragmentation correction is defined as the ratio

$$\delta^{(n)}_{fra}(y) = \frac{N^{(n)}_{par}(y)}{N^{(n)}_{had}(y)} \tag{10}$$

between the number of γ+n-jet events selected in the analysis before and after the simulation of the parton fragmentation. At the parton level the photon isolation criterion requires that no partons are generated at angles smaller than 20° to the photon.

Compared with the acceptance correction, the fragmentation correction is more delicate. In this case one cannot rely entirely on JETSET 7.3 PS because parton shower programs generate a larger number of partons (typically 7-8 in JETSET 7.3 PS) than the 2 or 3 partons considered in the $\mathcal{O}(\alpha, \alpha_s)$ matrix element.

Therefore three different approaches are used to evaluate $\delta^{(n)}_{fra}(y)$:

1. The first estimate is obtained from JETSET 7.3 PS, by comparing the jet multiplicity distributions before and after the string fragmentation has been applied.
2. In the second approach JETSET 7.3 PS is used again, but in this case only the two quarks and the first emitted gluon are considered for the jet definition and for the photon isolation condition. The correction is then obtained by comparing the jet rates obtained by applying the analysis on these three partons and on the final hadrons.
3. A third approach consists in interfacing the EEPRAD and GNJETS generators with the Lund string fragmentation routines and then comparing the jet rates before and after the simulation of the hadronization process.

The comparison of the three methods provides an estimate of how the correction factor depends on the generated parton multiplicity.

The correction factors obtained as a function of the resolution parameter y are shown in fig. 5, where the four curves correspond respectively to the original JETSET 7.3 PS

prediction, to the 3-parton cascade version of JETSET, and to the two ME generators with string fragmentation. For the final evaluation of $\delta^{(n)}_{fra}(y)$ the average of the four curves is used, with a systematic uncertainty equal to their R.M.S. spread.

The correction factors $\delta^{(n)}_{acc}(y)$ and $\delta^{(n)}_{fra}(y)$ applied to the data are reported as a function of y and of the jet multiplicity in Table 1.

7 Comparison with $\mathcal{O}(\alpha, \alpha_s)$ matrix element predictions

In $\mathcal{O}(\alpha, \alpha_s)$ matrix element predictions the production cross section for final state photons depends on two external parameters:

- The coupling of up-type and down-type quarks to the Z^0 boson. Specifically, by changing the relative amounts of up-type and down-type quarks in the hadronic sample, the rate of FSR radiation may be enhanced or suppressed.
- The value of $\alpha_s^{(1)}$, where the superscript '(1)' refers to the fact that the coupling constant is evaluated at first order in QCD. This is because, once a hard gluon is radiated, there is less energy available for a hard photon as well. Therefore a large value for $\alpha_s^{(1)}$ tends to suppress photon radiation.

For the comparison presented in this section the Standard Model predictions are assumed for the electroweak couplings of quarks.

As a preliminary check of the relative normalization of EEPRAD and GNJETS predictions, the strong coupling constant is initially set equal to zero in both generators in order to switch off the QCD corrections. The two estimates agree to within 0.5% (independent of y) in the predictions for the γ+1-jet and γ+2-jet rates with $\alpha_s^{(1)} = 0$.

7.1 Measurement of $\alpha_s^{(1)}$

As suggested in reference [6], an estimate of $\alpha_s^{(1)}$ which is independent of the absolute normalization can be derived from the fraction $f_3(y)$ of γ+3-jet events in the data. This is achieved by fitting the observed ratio

$$R_{3,2}(y) = \frac{\Gamma(\gamma + 3 \text{ jets})(y)}{\Gamma(\gamma + 2 \text{ jets})(y) + \Gamma(\gamma + 3 \text{ jets})(y)}. \tag{11}$$

The value of $\alpha_s^{(1)}$ extracted from the data as a function of y is shown in fig. 6. The variation of $\alpha_s^{(1)}$ with y is no larger than expected from its statistical and systematic uncertainty. The measured values of $\alpha_s^{(1)}$ are also reported in Table 2. It should be noted that such values cannot be compared directly with second order $\alpha_s^{(2)}$ measurements at LEP [26].

In principle, any value of y could be used for the determination of $\alpha_s^{(1)}$. However, small values ($y \leq 0.01$) should be avoided because of the large 3-jet (and 4-jet) rate which requires higher order QCD calculations. On the other hand, large values of y are affected by large statistical uncertainties. In order to provide a reasonable standard for comparison, the value at $y = 0.02$, namely $\alpha_s^{(1)} = 0.186 \pm 0.020$, is adopted as an input to the ME calculations.

7.2 Systematic uncertainties on the matrix element predictions

To evaluate the uncertainty in the ME predictions, two parameters are varied in the Monte Carlo generators: the so-called y_0 cut-off [7] and the degree of isolation for FSR photons.

In the EEPRAD and GNJETS generators the y_0 cut-off is introduced in order to isolate the quark-gluon soft and collinear singularity in the phase space integration of the $\mathcal{O}(\alpha, \alpha_s)$ matrix element. In both algorithms y_0 is expressed as a minimum two-parton scaled invariant mass:

$$y_0 = y_{qg}^{min} = \left(\frac{m_{qg}^{min}}{M_Z} \right)^2 . \tag{12}$$

Since y_0 is a non-physical parameter, the predicted cross section should not change when its value is varied within a reasonable range [10]. As a consequence, the uncertainty associated with the theoretical predictions must include at least the residual dependence of the FSR cross section on the choice of y_0. For the comparison presented in this analysis the y_0 parameter is varied in the range $10^{-4}y < y_0 < 10^{-2}y$ for EEPRAD and $5 \cdot 10^{-7} < y_0 < 10^{-5}$ for GNJETS. The different ranges considered follow the suggestions of the authors. They arise from the different algorithms used by the two programs in the treatment of the quark-gluon singularity.

A second source of theoretical uncertainty is the possibility that the 20° isolation condition is violated by soft hadronic particles. Specifically, the maximum amount of hadronic energy inside the isolation cone is allowed to vary between zero (complete isolation) and 500 MeV. The reason for this additional uncertainty is that in the ME approach small amounts of energy, up to several hundred MeV, cannot be precisely reproduced, although they can induce a non-negligible effect on the FSR cross section because of the isolation condition.

The overall systematic uncertainty assigned to the ME predictions for each value of y can be found in Tables 3-5.

7.3 Final results

The corrected distributions

$$f_n(y) = f_n^{exp}(y) \cdot \delta_{acc}^{(n)}(y) \cdot \delta_{fra}^{(n)}(y) \tag{13}$$

for the final comparison with EEPRAD and GNJETS predictions, are shown in Tables 3-5 and in figs. 7-9. The value $\alpha_s^{(1)} = 0.186 \pm 0.020$ is assumed for the ME predictions. The uncertainty associated to the ME predictions shown in figs. 7-9 includes the systematic uncertainty described above and the variation of $\alpha_s^{(1)}$.

Despite the use of a relatively large value for $\alpha_s^{(1)}$, as suggested by the relative jet fractions (Section 7.1), the ME predictions overestimate the photon yield, especially in the photon plus one jet case in the region of the jet resolution parameter y from 0.05 to 0.1, and in the photon plus two jet case for values of y around 0.1.

8 Measurement of the electroweak couplings

If all energetic isolated photons remaining after the cuts and after the background subtractions are attributed to the final state radiation of primary quarks, the electroweak

couplings of *up* and *down* quarks can be determined from the comparison of their production rate with the measured hadronic width of the Z^0. Following the notation of reference [16], the electroweak couplings of final state fermions are written as

$$c_f = v_f^2 + a_f^2 \tag{14}$$

where, in the Standard Model, the vector and axial couplings v and a are given by

$$v_f = 2I_{3,f} - 4Q_f \sin^2\theta_W \quad \text{and} \quad a_f = 2I_{3,f}. \tag{15}$$

In eqn. (15) I_3, Q and θ_W are the third component of the weak isospin, the charge of the quark, and the weak mixing angle, respectively.

Assuming that only five quark flavours contribute, the hadronic decay width of the Z^0 in second order QCD is given by

$$\Gamma_{had} = N_c \frac{G_\mu M_Z^3}{24\pi\sqrt{2}} \cdot (1 + \frac{\alpha_s^{(2)}}{\pi} + 1.41(\frac{\alpha_s^{(2)}}{\pi})^2) \cdot (3c_{1/3} + 2c_{2/3}) \tag{16}$$

where N_c is the number of colours, G_μ is the muon decay constant, M_Z is the mass of the Z^0 , and $\alpha_s^{(2)}$ is the strong coupling constant to second order QCD. The constants $c_{1/3}$ and $c_{2/3}$ are the couplings to charge 1/3 and charge 2/3 quarks respectively. The use of the latest parameter values from the DELPHI experiment [27], $M_Z = 91.187 \pm 0.009$ GeV, $\Gamma_{had} = 1.725 \pm 0.012$ GeV, and $\alpha_s^{(2)} = 0.123 \pm 0.005$ leads to

$$S_{q\bar{q}} = (3c_{1/3} + 2c_{2/3}) = 6.66 \pm 0.05, \tag{17}$$

with the uncertainty dominated by the contribution from the hadronic width.

The decay width into final state radiative events is proportional to a different linear combination of the coupling constants, $c_{1/3}$ and $c_{2/3}$. Since the photons couple to the square of the electric charge of the quarks, the yield of radiative events remaining after the cuts is proportional to $S_{\gamma q\bar{q}} = (3c_{1/3} + 8c_{2/3})$.

In the ME calculations the quarks are assumed to be massless. Including actual quark masses reduces the phase space for photon radiation, thus decreasing the FSR rate. In the case of the 5.2 GeV b-quark the difference may be noticeable. The L3 Collaboration has studied the effect of the b-quark mass [5], using a photon energy cut similar to the one used in this analysis. They suggest changing the expression for $S_{\gamma q\bar{q}}$ to $S_{\gamma q\bar{q}} = (3-\epsilon)c_{1/3}+8c_{2/3}$, in which $\epsilon = 0.2\pm0.1$.

By comparing the measured yield of γ+n-jet events (summing up the 1-jet, 2-jet and 3-jet contributions) with the two $\mathcal{O}(\alpha, \alpha_s)$ ME calculations at $y = 0.02$, where the predictions are believed to be most reliable (as for the measurement of $\alpha_s^{(1)}$), the value

$$S_{\gamma q\bar{q}} = 11.71 \pm 0.43 \pm 0.78 \pm 0.50 \pm 0.25 \tag{18}$$

is obtained. The first uncertainty is statistical, the second is systematic (experimental), the third is the theoretical uncertainty in the ME calculations, and the last corresponds to the variation of $\alpha_s^{(1)}$.

However, when values of y other than 0.02 are chosen, a significant variation in the result is observed. This strong dependence on y is taken into account by introducing an additional systematic error of $^{+1.07}_{-1.78}$, which corresponds to the variation of $S_{\gamma q\bar{q}}$ obtained by letting y vary in the range $0.01 < y < 0.06$. The upper value $y = 0.06$ is chosen in order to keep the contribution from γ+1-jet events below 30% of the total photon yield as the cross section of mono-jet events can be significantly sensitive to non-perturbative contributions which are neglected in the EEPRAD and GNJETS models [7].

Adopting the same correction as the L3 Collaboration for the b-quark mass effect and comparing with eqn. (17), the following values are obtained for the electroweak couplings:

$$c_{2/3} = v_{2/3}^2 + a_{2/3}^2 = 0.91^{+0.25}_{-0.36} \quad \text{and} \quad c_{1/3} = v_{1/3}^2 + a_{1/3}^2 = 1.62^{+0.24}_{-0.17}. \tag{19}$$

The result is compatible with the Standard Model expectation, $c_{2/3} = 1.1452 \pm 0.0008$ and $c_{1/3} = 1.4768 \pm 0.0007$, obtained by inserting the latest experimental value of $\sin^2\theta_W$ [28] into eqn. (15). It is also compatible with previous measurements of the couplings by other LEP experiments [5,6]. With the correction for the b-quark mass effect included, the Standard Model prediction for $S_{\gamma q\overline{q}}$ is 13.30 ± 0.15 and the DELPHI measurement, including all uncertainties, is $S_{\gamma q\overline{q}} = 11.7^{+1.5}_{-2.1}$.

9 Conclusions

In the $Z^0 \to q\overline{q}$ decays collected by DELPHI in 1991, 1992 and 1993 the cross section for producing isolated final state photons with energy $E_\gamma > 5.5$ GeV has been measured. After correcting for acceptance and fragmentation effects, the data have been compared, in terms of jet multiplicity, with the exact $\mathcal{O}(\alpha, \alpha_s)$ matrix element predictions provided by the two generators EEPRAD and GNJETS.

The comparison shows that in the matrix element the value $\alpha_s^{(1)} = 0.186 \pm 0.020$ has to be assumed for the (first order) strong coupling constant in order to reproduce the measured fraction of γ+3-jet events. With $\alpha_s^{(1)}$ set at the measured value, the ME predictions generally tend to overestimate the absolute photon yield.

By assuming the $\mathcal{O}(\alpha, \alpha_s)$ predictions at $y = 0.02$, where they are most reliable, as a reference for the Standard Model expectation, the values $c_{2/3} = 0.91^{+0.25}_{-0.36}$ and $c_{1/3} = 1.62^{+0.24}_{-0.17}$ have been derived for the electroweak couplings of charge 2/3 (u-type) and charge 1/3 (d-type) quarks to the Z^0 boson. The result is compatible with the Standard Model prediction.

Acknowledgements

We wish to thank E.W.N. Glover, A.G. Morgan, J.C. Thompson and H. Spiesberger for many useful discussions. We are greatly indebted to our technical collaborators and to the funding agencies for their support in building and operating the DELPHI detector, and to the members of the CERN-SL Division for the excellent performance of the LEP collider.

References

[1] *Proceedings of the Workshop on Photon Radiation from Quarks*, Annecy, 2-3 December 1991, CERN Report 92-04.

[2] E. Laermann, et al., Nucl. Phys. **B207** (1982) 205.

[3] D. Decamp, et al. (ALEPH Collaboration), Phys. Lett. **264B** (1991) 476;
D. Buskulic, et al. (ALEPH Collaboration), Zeitschr. Phys. **C57** (1993) 17.

[4] P. Abreu, et al. (DELPHI Collaboration), Zeitschr. Phys. **C53** (1992) 555.

[5] O. Adriani, et al. (L3 Collaboration), Phys. Lett. **292B** (1992) 472;
O. Adriani, et al. (L3 Collaboration), Phys. Lett. **301B** (1993) 136.

[6] M. Z. Akrawy, et al. (OPAL Collaboration), Phys. Lett. **246B** (1990) 285;
G. Alexander, et al. (OPAL Collaboration), Phys. Lett. **264B** (1991) 219;
P. D. Acton, et al. (OPAL Collaboration), Zeitschr. Phys. **C54** (1992) 193;
P. D. Acton, et al. (OPAL Collaboration), Zeitschr. Phys. **C58** (1993) 405;
R. Akers, et al. (OPAL Collaboration), "Comparisons of the Properties of Final State Photons in Hadronic Z^0 Decays with Predictions from Matrix Element Calculations", CERN–PPE/95–13, 3 February 1995.

[7] Z. Kunszt and Z. Troscanyi, Nucl. Phys. **B394** (1993) 139.

[8] K. Koller, et al., Zeitschr. Phys. **C2** (1979) 197.

[9] G. Kramer and B. Lampe, Phys. Lett. **B269** (1991) 401.

[10] P. Mättig, H. Spiesberger and W. Zeuner, Zeitschr. Phys. **C60** (1993) 613.

[11] E.W.N. Glover and W.J. Stirling, Phys. Lett. **B295** (1992) 128.

[12] G. Kramer and H. Spiesberger, in ref. [1].

[13] T. Sjöstrand, Comp Phys. Comm. **39** (1986) 347;
T. Sjöstrand, "Pythia 5.6 and JETSET 7.3", CERN-TH/6488-92.

[14] U. Pettersson, LU/TP 88-5 (1988);
U. Pettersson and L. Lönnblad, LU/TP 88-15 (1988);
L. Lönnblad, Lund preprint LU/TP 89-10 (1989).

[15] G. Marchesini and B. R. Webber, Nucl.Phys **B238** (1984) 1;
B. R. Webber, Nucl.Phys **B238** (1984) 492;
G. Abbiendi, et al., Comp. Phys. Comm. **67** (1992) 465.

[16] P. Mättig and W. Zeuner, Zeitschr. Phys. **C52** (1991) 31.

[17] P. Aarnio, et al. (DELPHI Collaboration), Nucl. Instr. and Meth. **A303** (1991) 233.

[18] H.G. Fischer, Nucl. Instr. and Meth., **A265** (1988) 218;
F.L. Navarria, et al., Nucl. Instr. and Meth., **A257** (1987) 499;
A. Cattai, et al., Nucl. Instr. and Meth., **A235** (1985) 310;
E.I. Rosenberg, "The DELPHI High Density Projection Chamber", in *Proceedings of the Gas Sampling Calorimetry Workshop II*, Fermilab, Batavia, Il. (1985) 450;
H.G. Fischer and O. Ullaland, IEEE Trans. Nucl. Sci., **NS-27** (1980) 38;
A. Algeri, et al., CERN-PPE/95-04.

[19] H.B. Crawley, et al., IEEE Trans. Nucl. Sci., **NS-35** (1988) 295;
H.B. Crawley, et al., IEEE Trans. Nucl. Sci., **NS-34** (1987) 261.

[20] P. Checchia, et al., Nucl. Instr. and Meth. **A275** (1989) 49.

[21] DELSIM Reference Manual, DELPHI internal note, DELPHI 87-97 PROG-100.

[22] S. Catani, et al., Nucl. Phys. **B407** (1993) 3.

[23] J.E. Campagne and R. Zitoun, Zeitschr. Phys. **C43** (1989) 469.

[24] B. Andersson, et al., Phys. Rep. **97** (1983) 31.

[25] S. Jadach and Z. Was, Comp. Phys. Com. **36** (1985) 191;

S. Jadach, B.F.L. Ward and Z. Was, Comp. Phys. Com. **66** (1991) 276.

[26] The LEP Electroweak Working Group, *Combined preliminary data on Z parameters from the LEP experiments and constraints on the Standard Model*, CERN/PPE/94-187.

[27] P. Abreu, et al. (DELPHI Collaboration), Nucl. Phys. **B417** (1994) 3.

[28] D. Schaile, in *Proceedings of the XXVII International Conference in High Energy Physics*, Glasgow, July 20-27 1994, page 27.

y	$\gamma + 1\ jet$		$\gamma + 2\ jet$		$\gamma + 3\ jet$	
	δ_{acc}	δ_{fra}	δ_{acc}	δ_{fra}	δ_{acc}	δ_{fra}
0.01	1.09±0.06	0.69±0.25	1.78±0.10	1.10±0.09	2.59±0.15	1.17±0.23
0.02	1.12±0.06	0.91±0.12	1.72±0.10	1.08±0.05	2.76±0.16	1.10±0.20
0.03	1.20±0.07	1.02±0.09	1.79±0.10	1.07±0.04	2.43±0.14	1.10±0.16
0.04	1.27±0.07	1.06±0.09	1.85±0.11	1.06±0.05	2.42±0.14	1.10±0.16
0.05	1.29±0.07	1.07±0.05	1.93±0.11	1.05±0.04	2.22±0.13	1.20±0.07
0.06	1.41±0.08	1.06±0.04	1.96±0.11	1.06±0.04	2.79±0.16	1.07±0.12
0.07	1.43±0.08	1.07±0.05	1.88±0.11	1.06±0.04	2.50±0.14	1.20±0.05
0.08	1.43±0.08	1.07±0.04	1.94±0.11	1.06±0.03	3.42±0.20	1.73±0.64
0.09	1.43±0.08	1.09±0.04	1.93±0.11	1.07±0.02		
0.10	1.44±0.08	1.11±0.04	1.93±0.11	1.07±0.03		
0.11	1.42±0.08	1.12±0.05	2.10±0.12	1.05±0.05		
0.12	1.43±0.08	1.12±0.05	2.19±0.13	1.04±0.03		
0.13	1.45±0.08	1.14±0.05	2.30±0.13	1.05±0.05		
0.14	1.47±0.09	1.14±0.06	2.31±0.13	1.05±0.05		
0.15	1.53±0.09	1.14±0.05	2.33±0.13	1.06±0.07		
0.16	1.52±0.09	1.16±0.05	2.44±0.14	1.05±0.05		
0.17	1.54±0.09	1.14±0.05	2.39±0.14	1.07±0.04		
0.18	1.57±0.09	1.16±0.05	2.31±0.13	1.09±0.01		
0.19	1.53±0.09	1.17±0.04	2.41±0.14	1.05±0.02		
0.20	1.57±0.09	1.16±0.04	2.62±0.15	1.06±0.07		

Table 1: The acceptance ($\delta^{(n)}_{acc}(y)$) and fragmentation ($\delta^{(n)}_{fra}(y)$) correction factors applied to the experimental data for comparison with the predictions of EEPRAD and GNJETS. The uncertainty on the acceptance corrections originates from the photon selection criteria and the background subtraction. The uncertainty on the fragmentation correction is derived according to the method described in Section 6.2.2.

y	$\alpha_s^{(1)}$	
	EEPRAD	GNJETS
0.01	0.168±0.011	0.167±0.012
0.02	0.185±0.020	0.187±0.020
0.03	0.177±0.033	0.175±0.032
0.04	0.173±0.055	0.171±0.054
0.05	0.227±0.080	0.224±0.079
0.06	0.313±0.122	0.305±0.115

Table 2: Values of $\alpha_s^{(1)}$ measured in the isolated photon sample from the ratio $R_{3,2}(y) = \Gamma(\gamma + 3 \text{ jets})(y)/(\Gamma(\gamma + 2 \text{ jets})(y) + \Gamma(\gamma + 3 \text{ jets})(y))$. The uncertainty associated to the $\alpha_s^{(1)}$ determination includes statistical and systematic effects.

y	Corrected data	EEPRAD $\alpha_s^{(1)} = 0.186$	GNJETS $\alpha_s^{(1)} = 0.186$
0.01	3.6±0.7±1.3	9.6±2.7±1.6	5.8±1.2±2.0
0.02	7.6±1.3±1.1	15.3±3.5±2.0	11.1±2.2±2.5
0.03	11.9±1.7±1.3	20.8±4.3±2.3	16.2±2.5±2.8
0.04	15.3±2.0±1.5	26.1±4.0±2.4	21.1±2.9±3.0
0.05	17.8±2.2±1.4	31.1±4.2±2.5	25.7±3.5±3.1
0.06	21.3±2.5±1.5	35.7±3.6±2.7	30.0±4.1±3.3
0.07	23.9±2.6±1.8	40.0±4.7±2.7	34.0±5.2±3.4
0.08	26.0±2.7±1.8	44.0±4.5±2.9	37.7±5.4±3.6
0.09	30.0±2.8±2.1	47.6±3.8±3.0	41.1±5.7±3.7
0.10	33.6±3.0±2.3	50.8±4.0±3.2	44.1±6.0±3.9
0.11	37.1±3.0±2.7	53.8±4.2±3.3	46.9±6.2±4.1
0.12	39.1±3.1±2.9	56.8±3.9±3.5	49.8±6.2±4.3
0.13	42.0±3.3±3.1	60.0±3.3±3.7	52.7±6.6±4.5
0.14	43.9±3.4±3.3	63.3±3.8±3.8	55.7±7.3±4.7
0.15	48.3±3.6±3.5	66.7±4.0±3.9	58.9±7.1±4.8
0.16	50.8±3.6±3.8	70.3±3.9±4.0	62.1±8.1±4.9
0.17	52.8±3.7±3.7	74.0±6.4±4.1	65.5±8.1±5.0
0.18	55.4±3.9±3.9	77.9±3.7±4.1	68.9±8.9±5.2
0.19	55.7±3.8±3.8	81.9±4.3±4.1	72.4±9.6±5.2
0.20	59.0±3.9±4.1	86.1±5.6±4.1	76.1±10.1±5.3

Table 3: Final values for $f_1(y)\cdot 10^5$ observed in the data and in the predictions of EEPRAD and GNJETS with $\alpha_s^{(1)} = 0.186 \pm 0.020$. For the data the first error is statistical, the second is systematic. For the matrix element prediction the first error is statistical and systematic (combined), the second corresponds to the variation of $\alpha_s^{(1)}$.

y	Corrected data	EEPRAD $\alpha_s^{(1)} = 0.186$	GNJETS $\alpha_s^{(1)} = 0.186$
0.01	178.4±6.3±18.4	181.2±12.1±13.6	179.4±15.5±13.7
0.02	135.7±5.2±10.1	153.8±7.2±5.1	154.8±7.8±5.0
0.03	108.8±4.5±7.5	131.7±2.0±1.9	128.5±5.4±2.2
0.04	87.8±4.1±6.3	110.7±1.4±0.7	108.6±3.6±1.0
0.05	74.8±3.7±5.3	93.6±2.4±0.3	92.0±2.5±0.4
0.06	62.8±3.5±4.2	80.1±1.3±0.1	78.6±2.1±0.1
0.07	50.5±3.1±3.5	68.9±0.6±0.2	67.9±1.7±0.1
0.08	44.0±3.0±2.9	59.4±1.7±0.3	58.7±1.9±0.2
0.09	37.0±2.7±2.3	51.0±0.8±0.3	50.6±1.6±0.3
0.10	30.1±2.5±1.9	44.8±1.0±0.3	43.8±1.2±0.3
0.11	24.7±2.5±1.8	38.9±0.4±0.3	38.1±0.9±0.3
0.12	22.6±2.4±1.4	33.0±0.5±0.2	32.8±1.2±0.2
0.13	20.7±2.3±1.5	28.4±0.9±0.2	28.7±0.7±0.2
0.14	18.8±2.2±1.4	24.8±0.4±0.2	24.7±0.7±0.2
0.15	16.5±2.0±1.4	21.8±0.3±0.2	21.3±0.7±0.2
0.16	15.8±2.0±1.2	18.3±0.3±0.2	18.2±0.5±0.2
0.17	13.9±1.8±0.9	16.0±0.3±0.2	15.5±0.5±0.1
0.18	11.1±1.6±0.6	13.3±0.2±0.1	13.0±0.6±0.1
0.19	9.3±1.4±0.6	11.5±0.3±0.1	11.0±0.5±0.1
0.20	8.9±1.5±0.8	9.4±0.1±0.1	9.2±0.5±0.1

Table 4: As in Table 3 but for $f_2(y) \cdot 10^5$.

y	Corrected data	EEPRAD $\alpha_s^{(1)} = 0.186$	GNJETS $\alpha_s^{(1)} = 0.186$
0.01	61.0±4.8±12.5	73.3±0.0±7.9	73.0±0.2±7.9
0.02	21.2±2.7±4.0	24.3±0.0±2.6	24.0±0.2±2.6
0.03	8.2±1.7±1.3	10.5±0.0±1.1	10.4±0.1±1.1
0.04	3.7±1.2±0.6	5.0±0.0±0.5	5.0±0.0±0.5
0.05	2.4±0.9±0.2	2.5±0.0±0.3	2.5±0.0±0.3
0.06	1.6±0.6±0.2	1.3±0.0±0.1	1.2±0.0±0.1
0.07	1.0±0.5±0.1	0.6±0.0±0.1	0.6±0.0±0.1
0.08	0.8±0.6±0.3	0.3±0.0±0.0	0.3±0.0±0.0

Table 5: As in Table 3 but for $f_3(y) \cdot 10^5$.

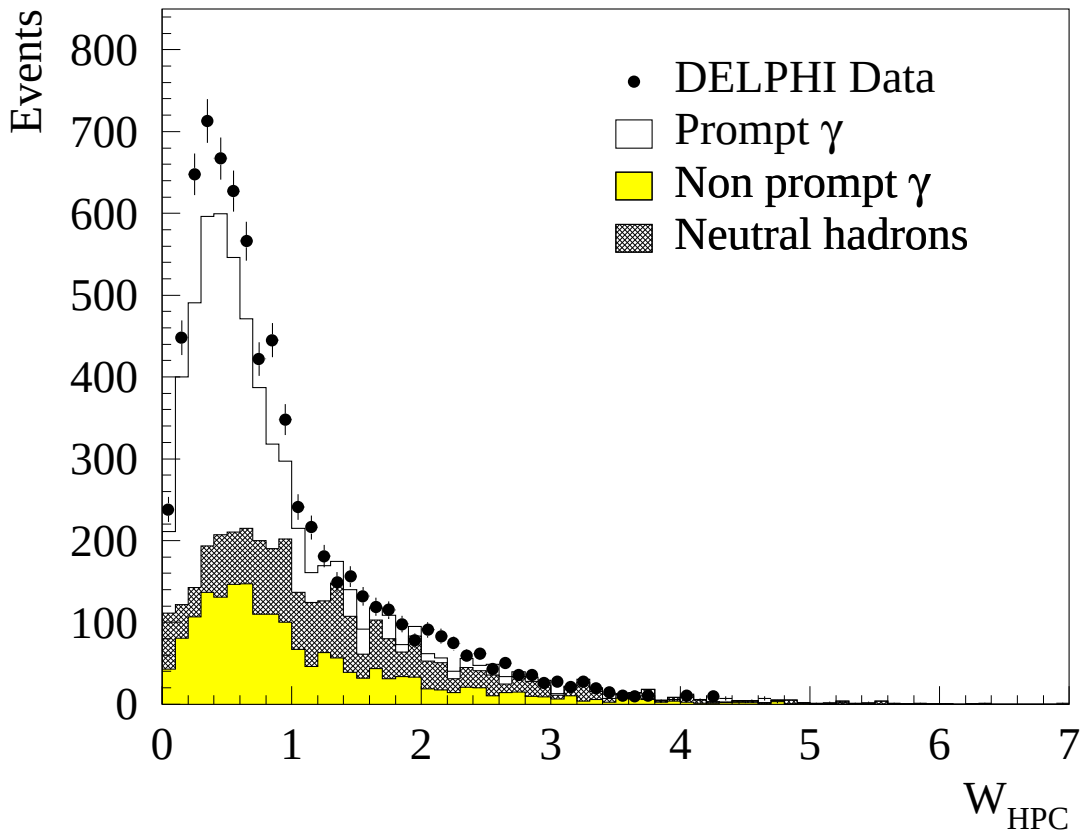

Figure 1: Distribution of the W_{HPC} parameter for the sample of isolated neutral clusters selected from real and simulated hadronic events. The simulation (based on JETSET 7.3 PS and DELSIM) is normalized according to the total integrated luminosity considered in the data. The prompt photon sample in the plot consists of FSR and ISR photons.

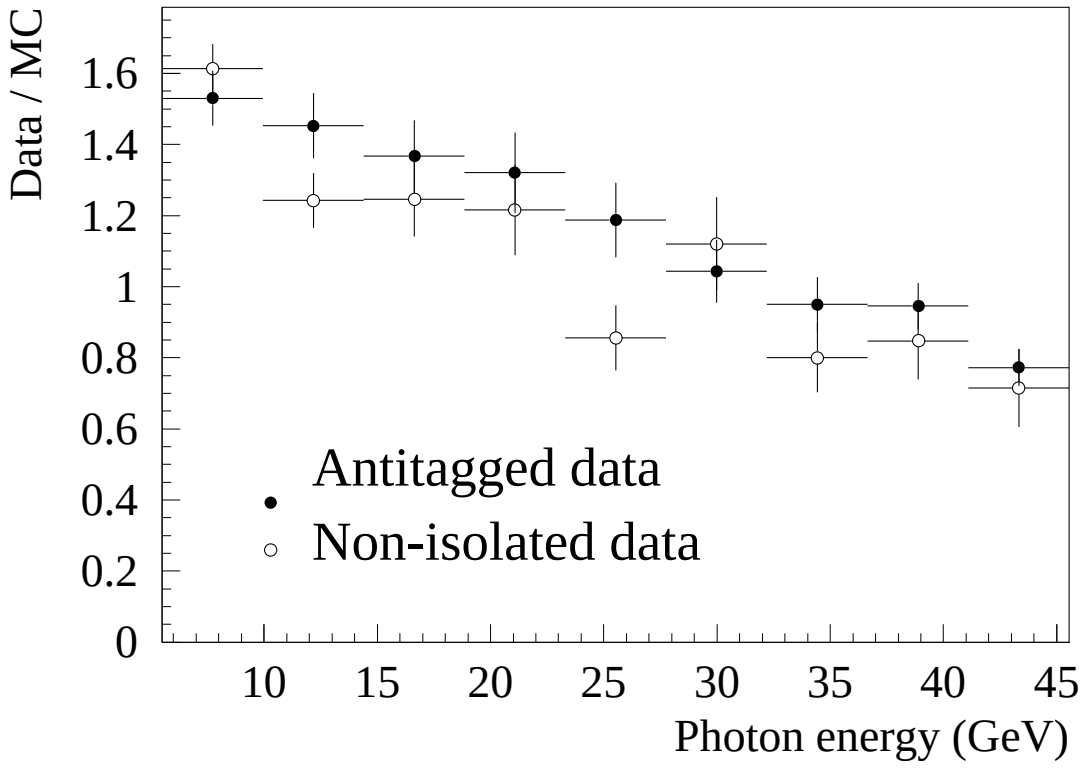

Figure 2: Ratio between real and simulated (JETSET 7.3 PS) event yields as a function of the shower energy in the two reference background samples.

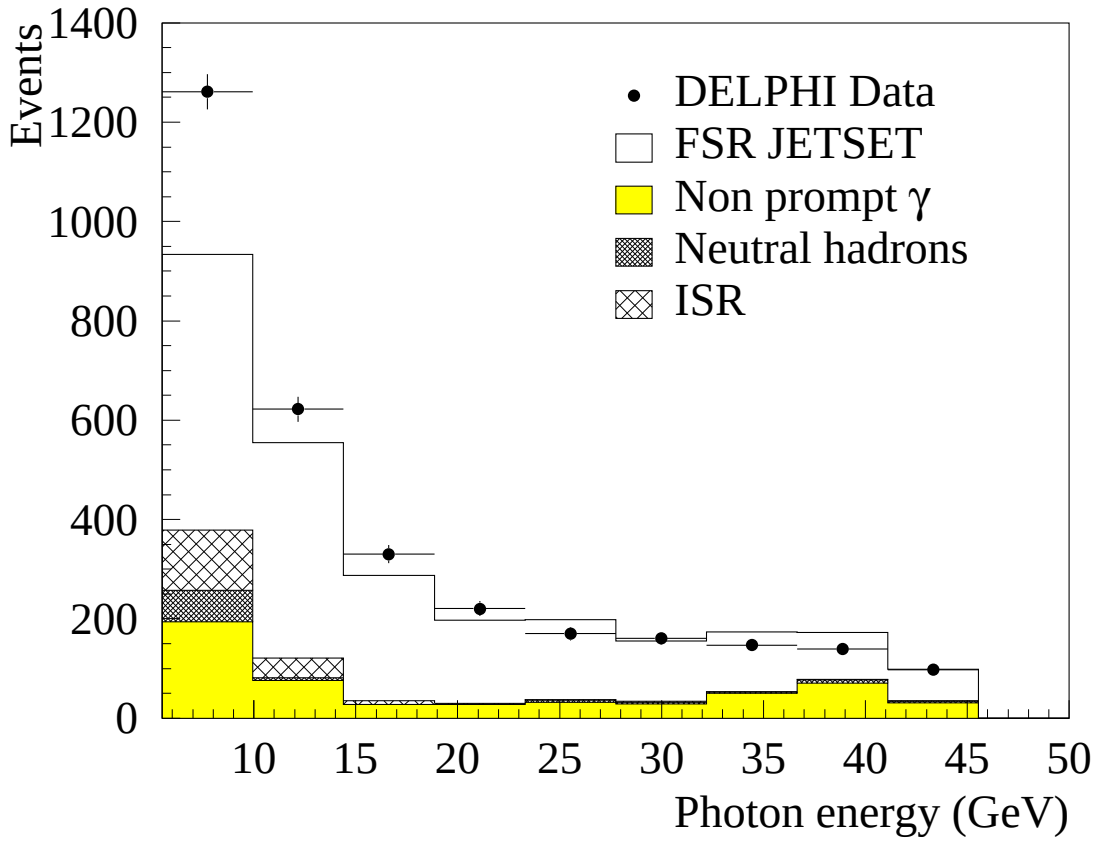

Figure 3: Comparison between the energy spectrum of isolated final state photons observed in the data and predicted by JETSET 7.3 PS. The background contaminations predicted by JETSET and DYMU3 have been rescaled according to the method described in Section 5. The plotted energy estimate is that obtained by means of the rescaling procedure described in Section 4.

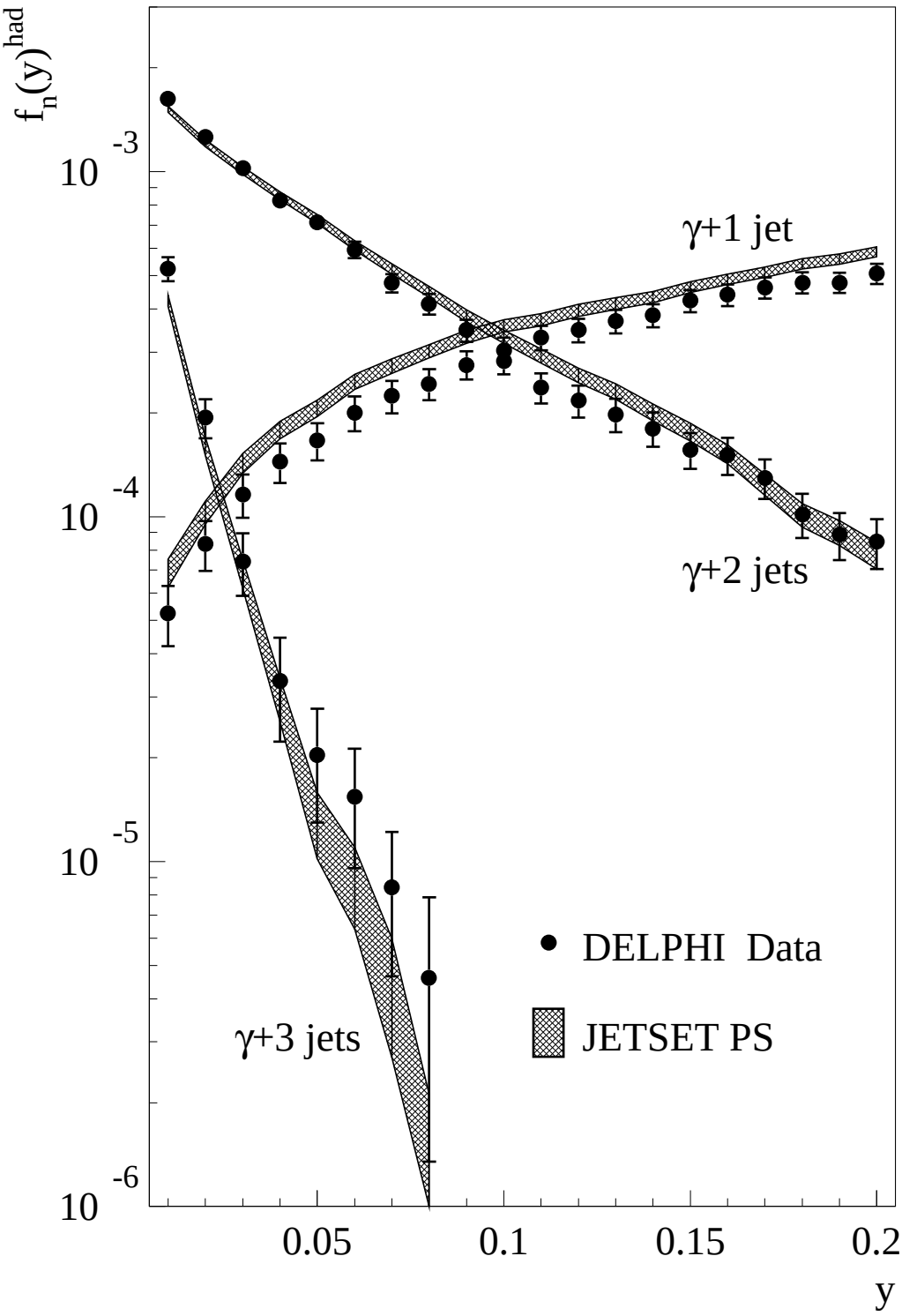

Figure 4: Comparison between the jet rates $f_n(y) = \Gamma(Z^0 \to \gamma + \text{n jets})/\Gamma(Z^0 \to q\overline{q})$ observed in the data and those predicted by the JETSET 7.3 PS model in events with an isolated photon. The comparison is carried out at the *hadron* level, i.e., after applying the acceptance correction but before applying the fragmentation correction. The shaded bandwidths represent the statistical uncertainty in the calculation.

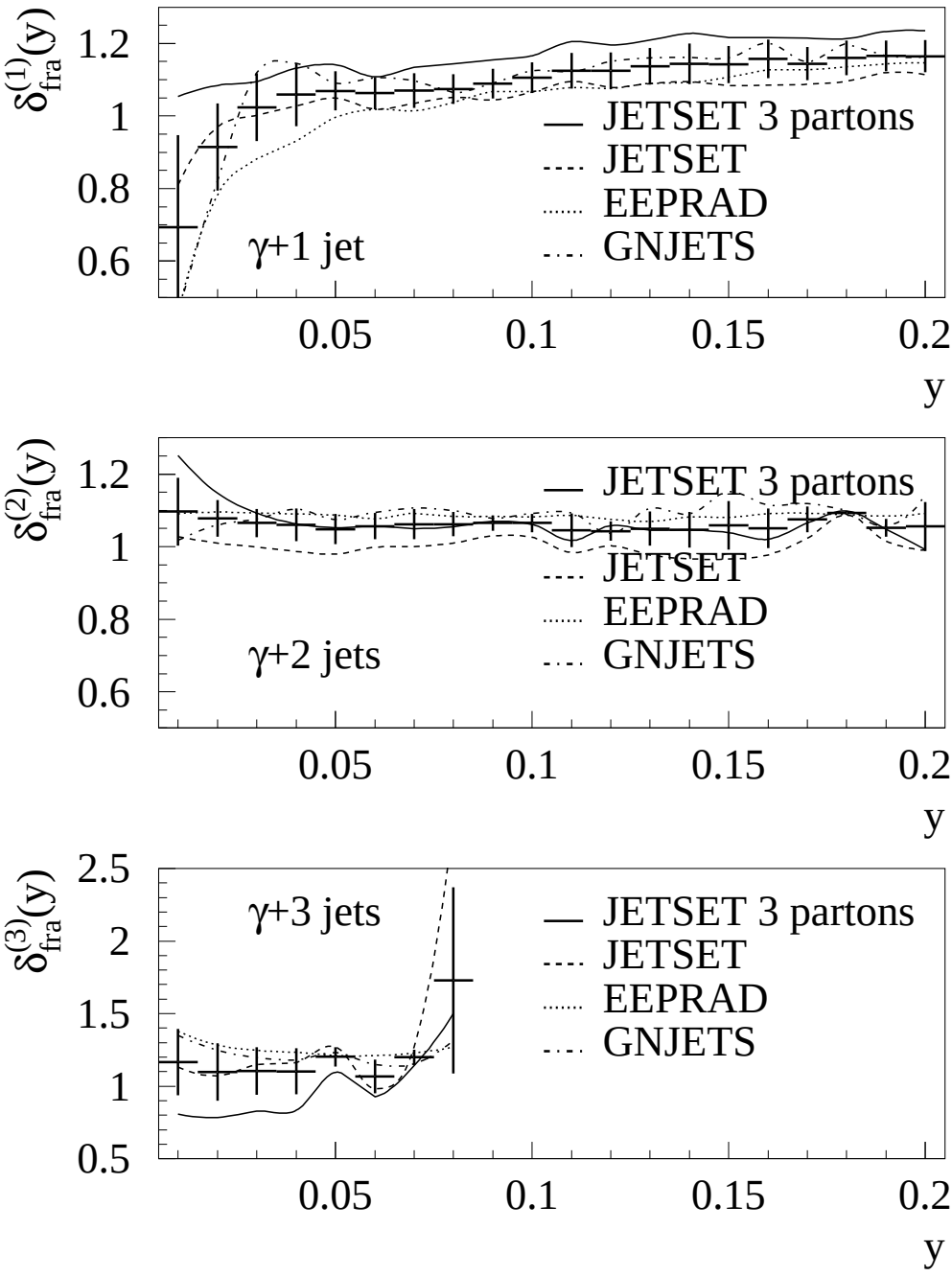

Figure 5: Estimates of the hadronization correction provided by JETSET 7.3 PS, EEPRAD and GNJETS with string fragmentation. For the final correction, which is represented by the points with error bars in the figure, the average of the four distributions is used with a systematic uncertainty equal to the R.M.S. spread.

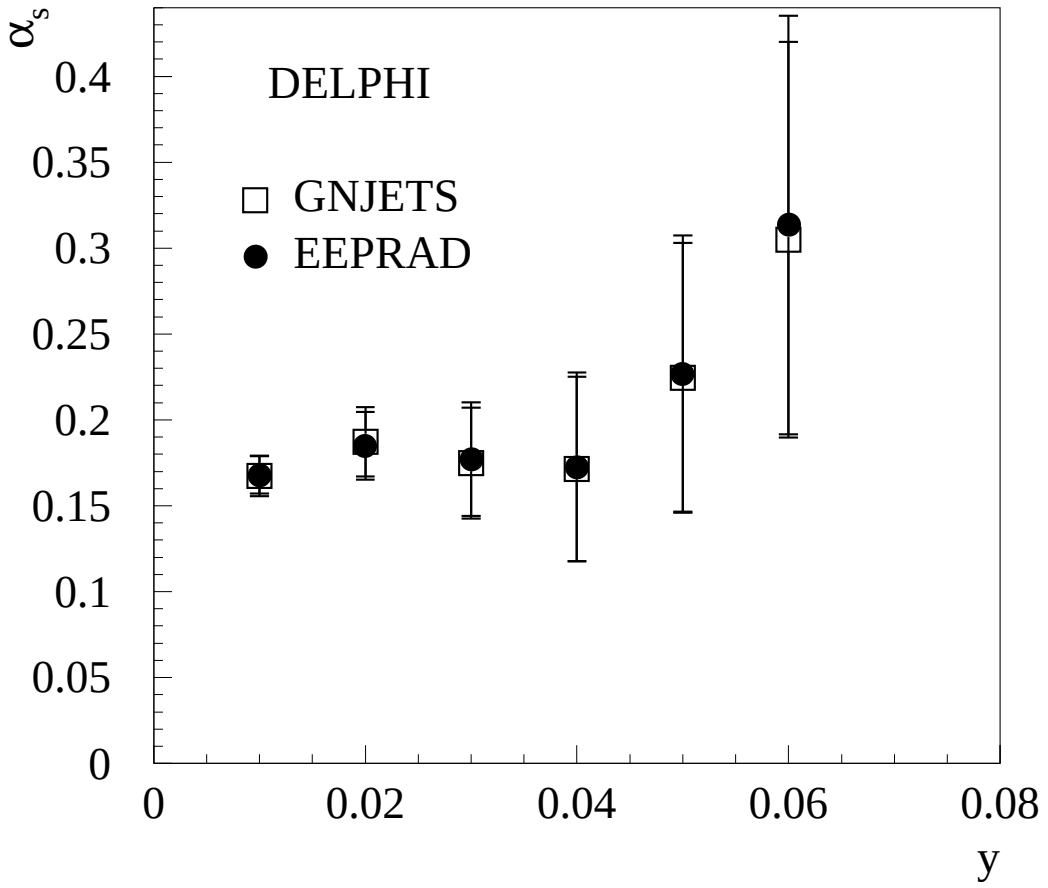

Figure 6: Values of $\alpha_s^{(1)}$ as measured in the isolated photon sample by comparing the ratio $R_{3,2}(y) = \Gamma(\gamma + 3\,\text{jets})(y)/(\Gamma(\gamma + 2\,\text{jets})(y) + \Gamma(\gamma + 3\,\text{jets})(y))$ with the prediction of EEPRAD and GNJETS.

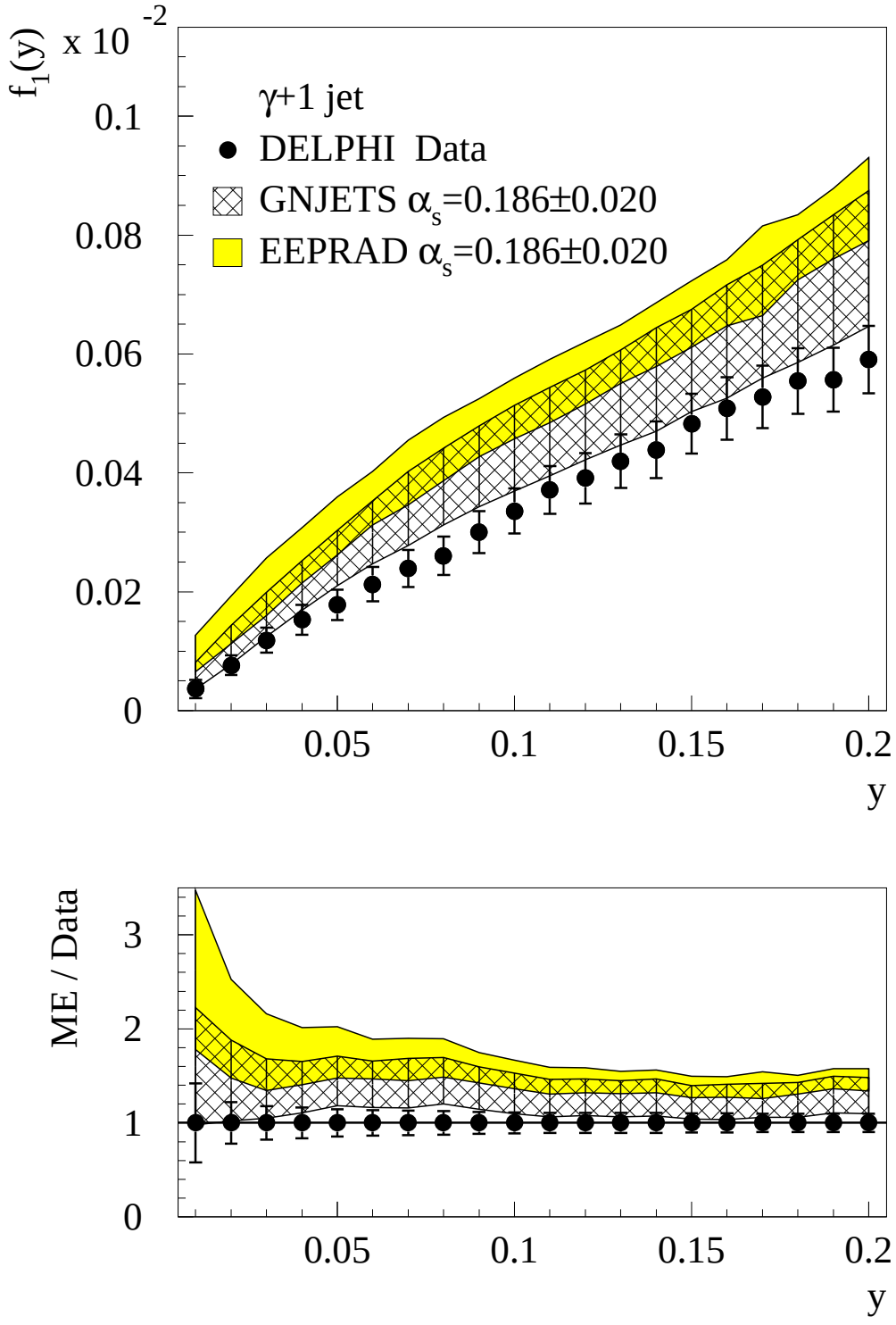

Figure 7: Top: The fraction $f_1 = \Gamma(Z^0 \to \gamma + 1 \text{ jet})/\Gamma(Z^0 \to q\overline{q})$ observed in the data and expected from EEPRAD and GNJETS as a function of the jet resolution parameter y. The uncertainty on the theoretical prediction includes the variation of $\alpha_s^{(1)}$ in the range $\alpha_s^{(1)} = 0.186 \pm 0.020$. Bottom: Ratio between the theoretical and the measured yields. The points in the bottom part of the figure are by definition unity, but they are displayed to show the relative uncertainties in the data.

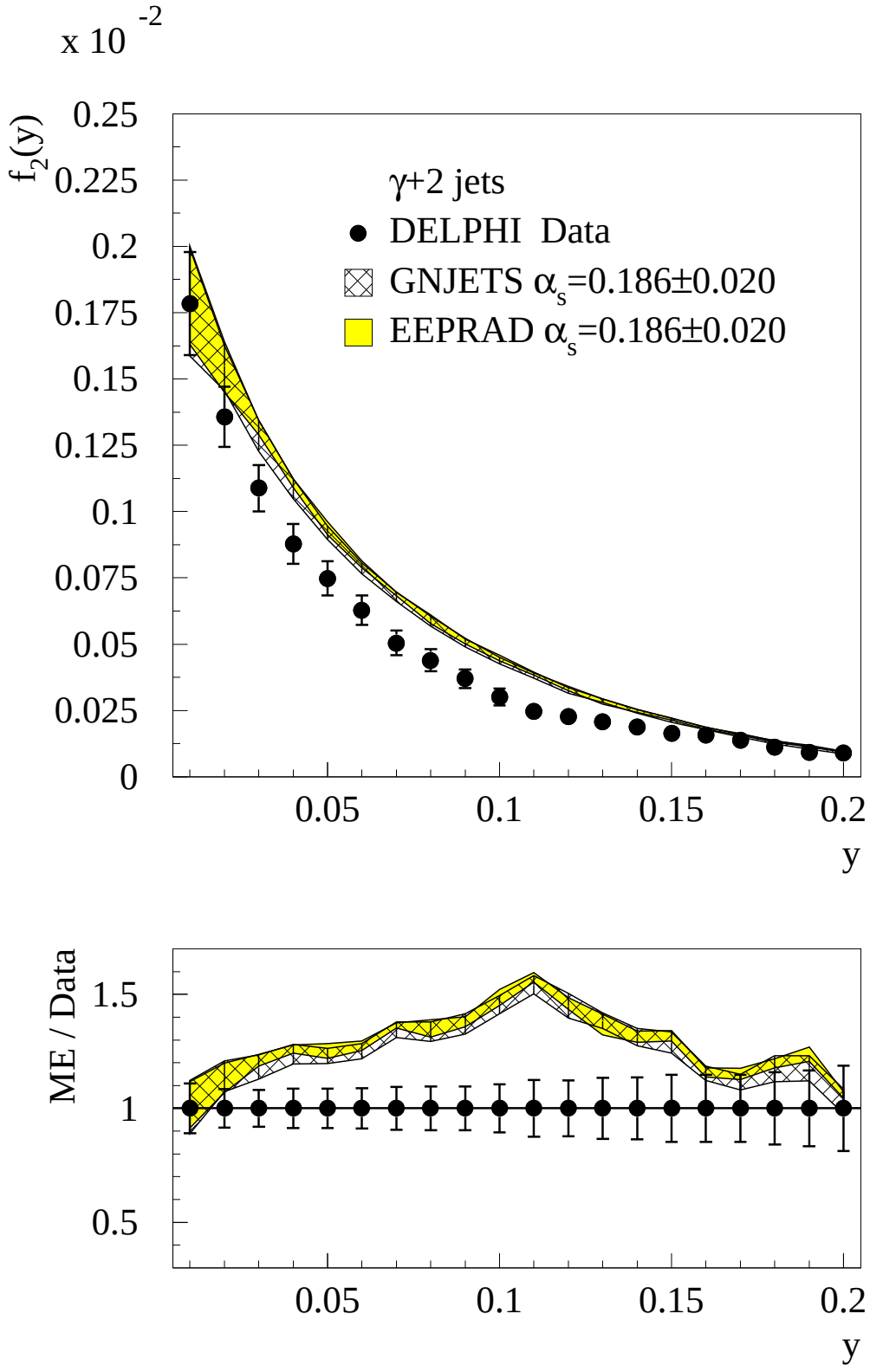

Figure 8: As in fig. 7 but for $f_2(y)$.

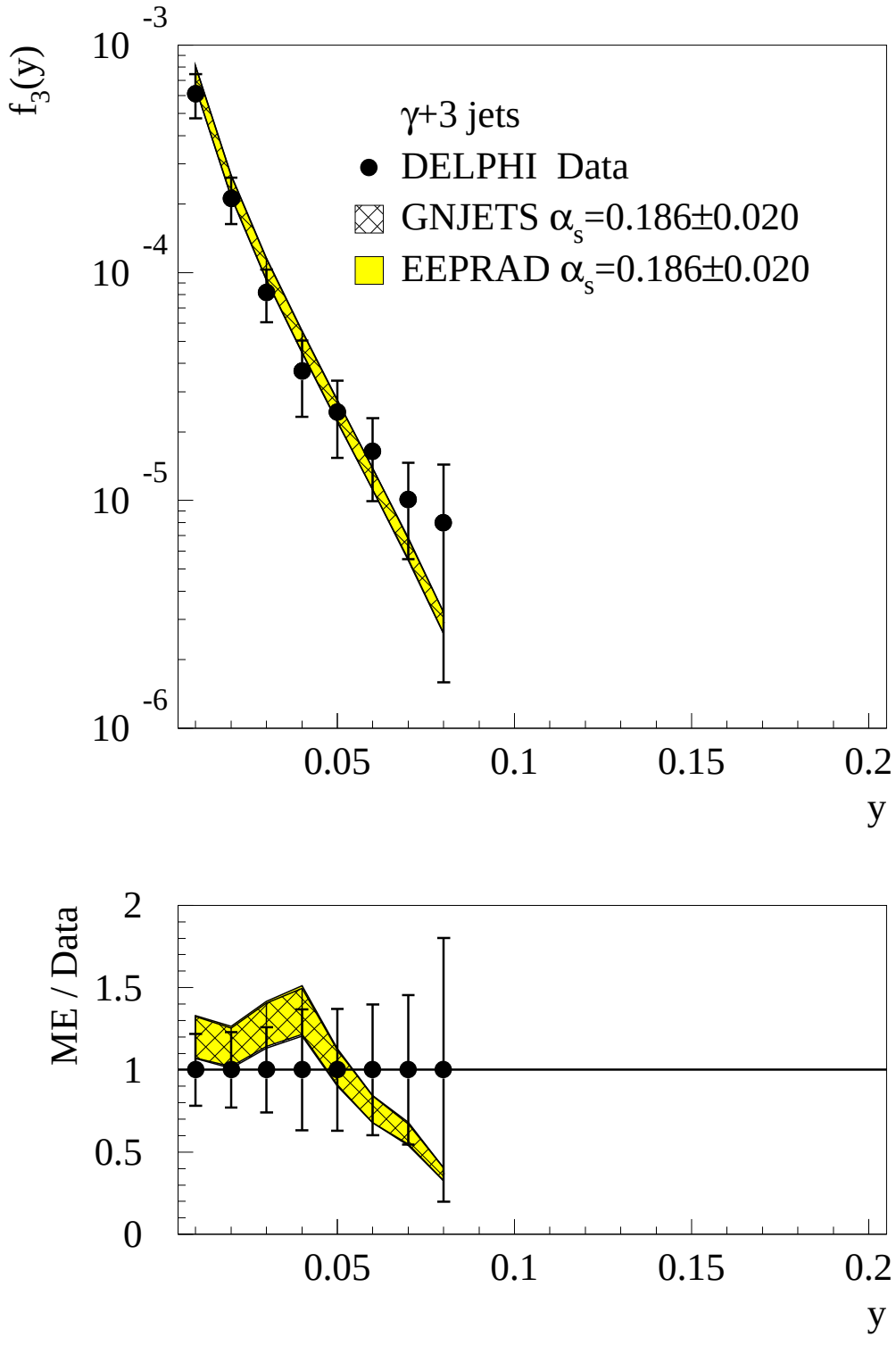

Figure 9: As in fig. 7 but for $f_3(y)$. The curves predicted by the two models are not distinguishable.